

## ALZHEIMER'S DISEASE

# Lateral mammillary body neurons in mouse brain are disproportionately vulnerable in Alzheimer's disease

Wen-Chin Huang<sup>1,2,†</sup>, Zhuyu Peng<sup>1,2,†</sup>, Mitchell H. Murdock<sup>1,2,†</sup>, Liwang Liu<sup>1,2</sup>, Hansruedi Mathys<sup>1,2,3,‡</sup>, Jose Davila-Velderrain<sup>3,4,§</sup>, Xueqiao Jiang<sup>1,2</sup>, Maggie Chen<sup>2</sup>, Ayesha P. Ng<sup>2</sup>, TaeHyun Kim<sup>1,2</sup>, Fatema Abdurrob<sup>1,2</sup>, Fan Gao<sup>1||</sup>, David A. Bennett<sup>5</sup>, Manolis Kellis<sup>3,4</sup>, Li-Huei Tsai<sup>1,2,3\*</sup>

Copyright © 2023 The Authors, some rights reserved; exclusive licensee American Association for the Advancement of Science. No claim to original U.S. Government Works

The neural circuits governing the induction and progression of neurodegeneration and memory impairment in Alzheimer's disease (AD) are incompletely understood. The mammillary body (MB), a subcortical node of the medial limbic circuit, is one of the first brain regions to exhibit amyloid deposition in the 5xFAD mouse model of AD. Amyloid burden in the MB correlates with pathological diagnosis of AD in human postmortem brain tissue. Whether and how MB neuronal circuitry contributes to neurodegeneration and memory deficits in AD are unknown. Using 5xFAD mice and postmortem MB samples from individuals with varying degrees of AD pathology, we identified two neuronal cell types in the MB harboring distinct electrophysiological properties and long-range projections: lateral neurons and medial neurons. Lateral MB neurons harbored aberrant hyperactivity and exhibited early neurodegeneration in 5xFAD mice compared with lateral MB neurons in wild-type littermates. Inducing hyperactivity in lateral MB neurons in wild-type mice impaired performance on memory tasks, whereas attenuating aberrant hyperactivity in lateral MB neurons ameliorated memory deficits in 5xFAD mice. Our findings suggest that neurodegeneration may be a result of genetically distinct, projection-specific cellular dysfunction and that dysregulated lateral MB neurons may be causally linked to memory deficits in AD.

## INTRODUCTION

Neurodegeneration is a major cause of memory loss and cognitive impairment, but the mechanisms driving susceptibility to cell death in individual neurons of the degenerating brain are incompletely understood. Alzheimer's disease (AD) is a memory disorder pathologically characterized by extracellular deposits of amyloid plaques and neurofibrillary tangles (1–3), and evidence from human and animal studies indicates that AD impairs circuit connectivity and network function (1, 4–7). Neuronal hyperactivity, including non-convulsive seizure activity in the cortical and hippocampal networks (8–10), is evident in early stages of AD (4, 5, 11) even before amyloid plaque deposition (11, 12). Whereas neuronal hyperactivity and neurodegeneration in the cortical-hippocampal networks are associated with AD, memory systems are distributed throughout the brain (13–16), and contributions to AD dementia from deep brain regions are only vaguely characterized (17). Identifying new brain regions and cell types uniquely vulnerable to hyperexcitability, memory deficits, and neurodegeneration in AD may provide new therapeutic targets for disease-modifying treatments.

We recently examined the sequence of amyloid deposition in 5xFAD mice (18), a mouse model harboring five familial AD mutations that recapitulates AD-related cognitive and cellular dysfunctions (19). We found that the mammillary body (MB) exhibits the highest density of amyloid deposition (18). The MB is a subcortical node of the medial limbic circuit that plays a key role in memory retrieval (20, 21), and lesions in the MB result in anterograde amnesia and memory deficits (22–28). MB volume correlates with episodic memory recall in patients who underwent surgical removal of colloid cysts (25), in which the extent of MB atrophy differs among individuals. The critical role played by the MB in memory recall is recapitulated in lesion studies in monkeys (29–31), rats (32–40), and mice (41–44). Postmortem brain studies report amyloid deposition and neurofibrillary tangles in the MBs of individuals with AD (45–47) and suggest that increased MB amyloid is associated with increased likelihood of pathological AD (18). Moreover, MB synaptic alterations are observed before amyloid and neurofibrillary tangle pathology emerge (48), indicating that MB synaptic deficits may be an early event leading to disease progression. Reduction of MB volume is also reported in individuals with mild AD (49). Together, these findings suggest a potential role of MB dysfunction in early stages of AD, but whether and how MB circuit dysfunction is related to AD-related cognitive decline are unclear. Here, using single-cell transcriptomic profiling of mouse and human MB postmortem tissue, combined with multiple interventions in the 5xFAD mouse model of AD, we provide evidence that a class of MB neurons may be critically involved in AD memory loss.

<sup>1</sup>Picower Institute for Learning and Memory, Massachusetts Institute of Technology, Cambridge, MA 02139, USA. <sup>2</sup>Department of Brain and Cognitive Sciences, Massachusetts Institute of Technology, Cambridge, MA 02139, USA. <sup>3</sup>Broad Institute of MIT and Harvard, Cambridge, MA 02139, USA. <sup>4</sup>MIT Computer Science and Artificial Intelligence Laboratory, Cambridge, MA 02139, USA. <sup>5</sup>Rush Alzheimer's Disease Center, Rush University Medical Center, Chicago, IL 60612, USA.

†These authors contributed equally to this work.

‡Present address: University of Pittsburgh Brain Institute and Department of Neurobiology, University of Pittsburgh School of Medicine, Pittsburgh, PA 15213, USA.

§Present address: Human Technopole, Viale Rita Levi-Montalcini 1, Milan 20157, Italy.

||Present address: Caltech Bioinformatics Resource Center, Beckman Institute at Caltech, Pasadena, CA 91125, USA.

\*Corresponding author. Email: lhtsai@mit.edu

**RESULTS****Single-cell transcriptomic profiling of mouse MB brain tissue**

To define cell types in the MB of 5xFAD mouse brain, we dissected the hypothalamus, which includes the MB, for single-cell RNA sequencing (scRNA-seq) (fig. S1A). We pooled hypothalamus tissue from nine female C57BL/6 mice (2 months old) into two samples to reduce the variability of the dissected brain regions between samples. We included 7754 single cells for analysis, which we classified into astrocytes (expressing *Slc6a11*, *Agt*, and *Slc4a4*), microglia (*Aif1*, *Csf1r*, and *Cx3cr1*), neurons (*Snap25*, *Nrsn2*, and *Syt4*), mature oligodendrocytes (*Mag*, *Mal*, and *Mog*), oligodendrocyte precursor cells (*Pdgfra*, *Matn4*, and *C1ql1*), newly formed oligodendrocytes (*Fyn*, *Gpr17*, and *Bfsp2*), tanycytes (*Col23a1*, *Crym*, and *Rax*), ependymal cells (*Ccdc153*, *Tmem212*, and *Foxj1*), endothelial cells (*Cldn5*, *Itm2a*, and *Ly6c1*), and mural cells (*Vtn*, *Higd1b*, and *Ndufa4l2*) (fig. S1, B and C). All major cell types included cells derived from both samples (fig. S1D). Unsupervised clustering analysis of neurons ( $n = 1382$  cells) revealed 12 clusters (Fig. 1A). We classified neurons into glutamatergic and GABAergic neurons on the basis of the expression of genes necessary for the synthesis and packaging of glutamate and  $\gamma$ -aminobutyric acid (GABA) (Fig. 1B) (50). To evaluate which neuronal clusters represented MB neurons, we first determined whether MB neurons are glutamatergic or GABAergic using RNA in situ hybridization of *Slc17a6* and *Slc32a1*. We found expression of *Slc17a6* and the absence of *Slc32a1* in the mouse MB (Fig. 1C), indicating that the MB is composed of glutamatergic neurons, consistent with previous observations in rats (51, 52). Among the five glutamatergic neuronal clusters, the top marker genes for clusters 4 and 11 were detected in the MB (Fig. 1D), but the other clusters were not (fig. S2A), suggesting that clusters 4 ( $n = 154$  cells) and 11 ( $n = 47$  cells) represented two separate neuronal cell types in the MB. We found that the top marker genes for these two clusters (*Rprm* and *Tac2*) labeled neurons in anatomically discrete MB subregions, the medial MB (MM) and lateral MB (LM) (Fig. 1D). The expression profiles of LM and MM clusters revealed multiple discriminatory marker genes: MM marker genes included *Rprm*, *Cck*, *Cartpt*, *Lhx10s*, and *Foxb1*, whereas LM marker genes included *Tac2*, *Prlr*, *Esr1*, *Nr4a2*, and *Pdyn* (Fig. 1E). To interrogate the functional differences between these two types of neurons, we performed gene ontology (GO) enrichment analysis. The top GO terms for MM neurons were associated with ion channel activity (fig. S2B), whereas those for LM neurons included structural constituents of ribosomes (fig. S2C). These observations suggest that the two types of MB neurons may feature different electrophysiological properties and require specific metabolic demands. To confirm the transcriptional subtype of MB neurons, we microdissected the MB and repeated scRNA-seq in wild-type (WT) and 6-month-old 5xFAD mice (fig. S3). We again found consistent evidence for MM and LM neurons in the microdissected MB dataset in both WT and 5xFAD mice (fig. S3). Collectively, these findings indicate that neurons of the MB harbor two distinct neuronal subtypes.

**Two MB neuron subtypes are distinguished by morphology, projection targets, and neuronal activity patterns**

Given that the two types of MB neurons were located in anatomically defined subregions, we characterized their morphologies, projections, and neuronal activity patterns. To quantify neuronal morphology, we retro-orbitally injected AAV-PHP.eB-CAG-tdTomato (53) into female 2-month-old C57BL/6 mice to sparsely label MB neurons. We found that the somata of LM neurons were significantly ( $P = 0.0016$ ) larger than those of MM neurons (Fig. 2, A and B). Given that metabolic activity is associated with cell size (54, 55), this observation was consistent with our finding that LM neurons harbored elevated expression of genes associated with metabolic activity and protein synthesis compared with LM neurons (fig. S2C).

Given the differences in LM and MM neuronal soma size, we determined whether these neuronal types harbored different electrophysiological properties. Using cell-attached patch-clamp recordings, we found that MM neurons fired more action potentials than did LM neurons (Fig. 2C). The spontaneous firing rate was  $\sim 11$  Hz for MM neurons and  $\sim 0.2$  Hz for lateral MB neurons (Fig. 2D). The action potential threshold was much lower, and the width of action potentials was much shorter in MM neurons compared with LM neurons, whereas input resistance, resting membrane potential, and overshoot were not different between the two cell types (Fig. 2E). Action potentials are tightly regulated by sodium and potassium ion channels (56), and many genes encoding these channels, including subunits of sodium channels (*Scn1a* and *Scn1b*) and potassium channels (*Kcna2*), were enriched in MM neurons compared with LM neurons (table S1). Transcripts related to ion channels may therefore be responsible for the increased firing rate of MM compared with LM neurons.

To examine the projection patterns of MM and LM neurons, we began by using anterograde tracing. After injecting AAV8-CAMKII-eGFP into the MBs of female 2-month-old C57BL/6 mice (Fig. 2F), we found abundant axonal enhanced green fluorescent protein (eGFP) signals in the anterior thalamus (Fig. 2G) and the tegmental nuclei of Gudden (Fig. 2, H and I), consistent with previous neural tracing studies in rats and monkeys (51, 52, 57–59). To evaluate whether LM and MM neurons project to distinct brain regions, we performed retrograde tracing using cholera toxin subunit b (CTB), a recombinant protein that binds to ganglioside  $G_{M1}$  and mediates retrograde axonal transport, thereby labeling presynaptic neurons (60). Fluorophore-conjugated CTB injected into the medial and ventral (but not dorsal) regions of the anterior thalamus labeled presynaptic neurons in the medial (but not lateral) mouse MB (Fig. 2, J and K). In contrast, CTB injected into the anterior dorsal thalamic nucleus (one hemisphere) labeled presynaptic neurons located in the LM in both hemispheres (Fig. 2, L and M), suggesting that LM neurons project both ipsilaterally and contralaterally to the anterior dorsal thalamic nucleus. We also found that MM and LM neurons project to distinct nuclei within the tegmental nuclei of Gudden (fig. S4). These observations indicate that MM and LM neurons project to distinct brain regions.

**LM neurons in 5xFAD mice are more vulnerable to neurodegeneration compared with MM neurons**

On the basis of our observations that LM and MM neurons are distinct from one another across multiple dimensions, we

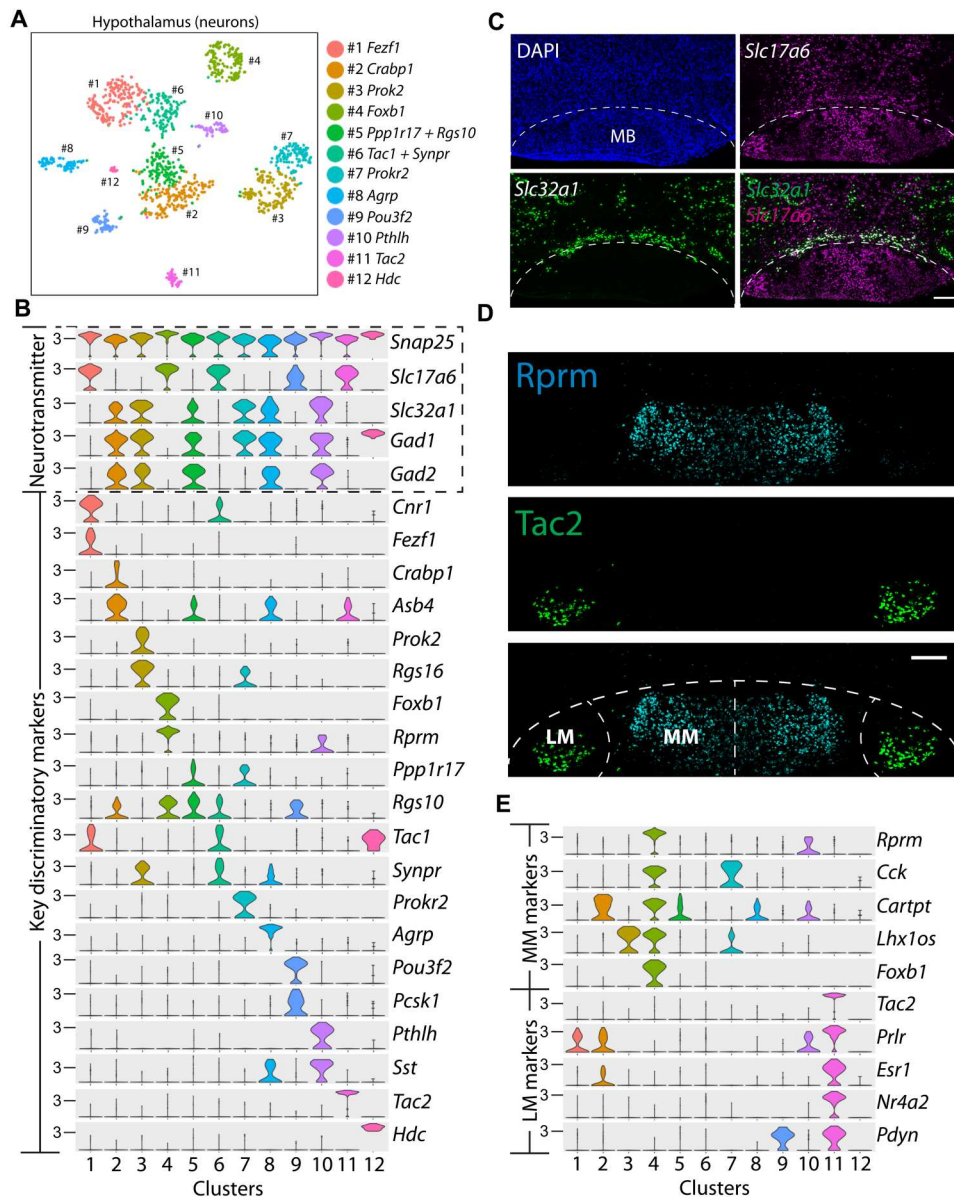


**Fig. 1. Single-cell transcriptomic analysis reveals two anatomically distinct neuronal cell types in the mouse MB.** (A) A *t*-distributed stochastic neighbor embedding (*t*-SNE) plot shows 12 clusters of neuronal subtypes in the hypothalami of C57BL/6 mice. (B) Violin plots demonstrate the expression of the pan-neuronal gene (*Snap25*), glutamatergic marker gene (*Slc17a6*), GABAergic marker genes (*Slc32a1*, *Gad1*, and *Gad2*), and the key discriminatory genes in each neuronal cluster. (C) Confocal images of WT mouse brain show in situ hybridization of *Slc17a6* (vesicular glutamate transporter 2; magenta) and *Slc32a1* (vesicular GABA transporter; green) in the MB, with 4',6-diamidino-2-phenylindole (DAPI) nuclear stain (blue). The dashed line outlines the boundary of the MB. Scale bar, 200  $\mu$ m. (D) Confocal image of in situ hybridization of *Tac2* (green) and *Rprm* (cyan) in the MBs of C57BL/6 WT mice. The dashed line outlines the boundary of the LM and MM. Scale bar, 200  $\mu$ m. (E) Violin plots show the expression of top marker genes for MM (cluster 4) and LM (cluster 11).

hypothesized they may be asymmetrically affected by AD. To explore this possibility, we used scRNA-seq from female 6-month-old 5xFAD mice and WT littermates, a time point when these mice suffer memory impairments (19). We pooled posterior hypothalami from four mice into one sample as one replicate and collected a total of three replicates per genotype (5xFAD and WT). We annotated 16,213 cells into major brain cell types (fig. S4, C and D), which were represented across biological replicates (fig. S5E) and genotypes (Fig. 3C and fig. S6). We confirmed our observation

that LM and MM neurons harbor distinct markers (Fig. 3A), including *Tac2* as a LM neuronal marker and *Rprm* as a MM neuronal marker (Fig. 3B).

To explore whether MM and LM neurons are differentially vulnerable to degeneration in 5xFAD mice, we performed in situ hybridization for MB marker genes in 6-month-old 5xFAD mice and WT control littermates. The density of *Tac2* neurons, a marker of LM neurons, was reduced in 5xFAD mice (Fig. 3, D and E), whereas the density of *Rprm* neurons, a marker of MM neurons, was not

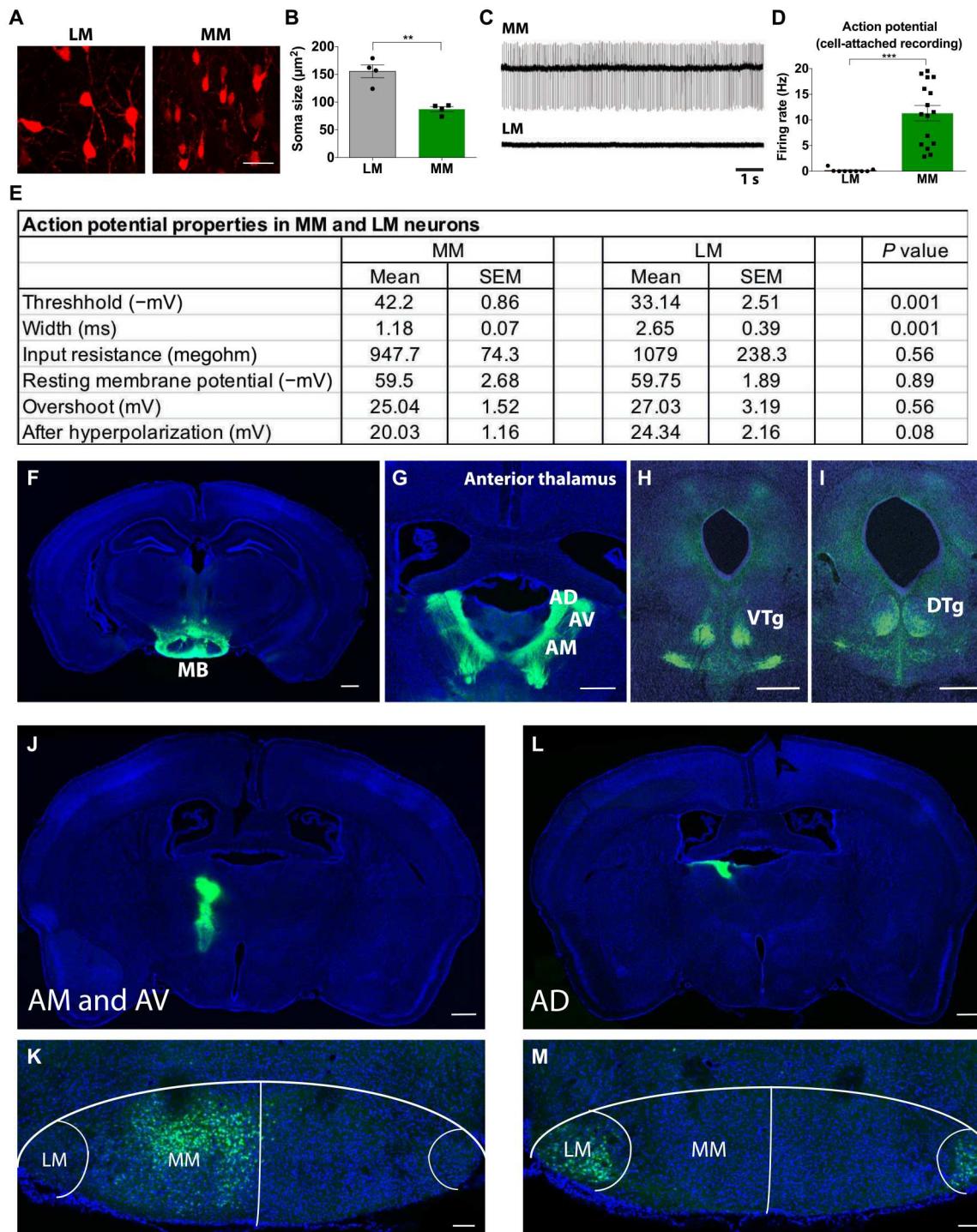


**Fig. 2. Mouse LM and MM neurons exhibit distinct morphologies, electrophysiological properties, and projection targets.** (A) Confocal images of mCherry-labeled neurons (red) in the LM and the MM are shown. Scale bar, 25  $\mu$ m. (B) Cell soma size for neurons in the LM and MM was measured.  $t(6) = 5.506$ ,  $P = 0.0015$ .  $**P < 0.01$  (unpaired  $t$  test).  $n = 4$  mice per group. (C) Representative action potential (AP) traces of neurons located in the MMs or LMs of WT mice are shown. (D) AP firing rate for MM neurons and LM neurons was quantified.  $t(23) = 5.490$ ,  $P < 0.0001$ .  $***P < 0.0001$  (unpaired  $t$  test).  $n = 9$  for LM and  $n = 16$  for MM neurons. (E) AP properties of MM and LM neurons are shown.  $n = 10$  to 12 cells per group ( $P$  values are shown; unpaired  $t$  test). (F to I) Representative images of mouse brain after injection of AAV8-CAMKII-eGFP into the MB. Images show (F) the MB projecting to (G) the anterior thalamus, including the anterior dorsal (AD), anterior medial (AM), as well as anterior ventral (AV) thalamic nuclei, (H) ventral tegmental nuclei (VTg), and (I) dorsal tegmental nuclei (DTg). DAPI stain (blue) and eGFP (green). Scale bars, 500  $\mu$ m. (J to M) Alexa Fluor 488 (green)-conjugated cholera toxin B (CTB) was injected into (J) AM and AV thalamic nuclei and (L) AD thalamic nuclei of WT mouse brains. CTB-labeled neurons (green) were located in (K) the MMs and (M) the LMs of mouse brain slices. Hoechst stain, blue. Scale bars, 500 (J and L) and 100  $\mu$ m (K and M).

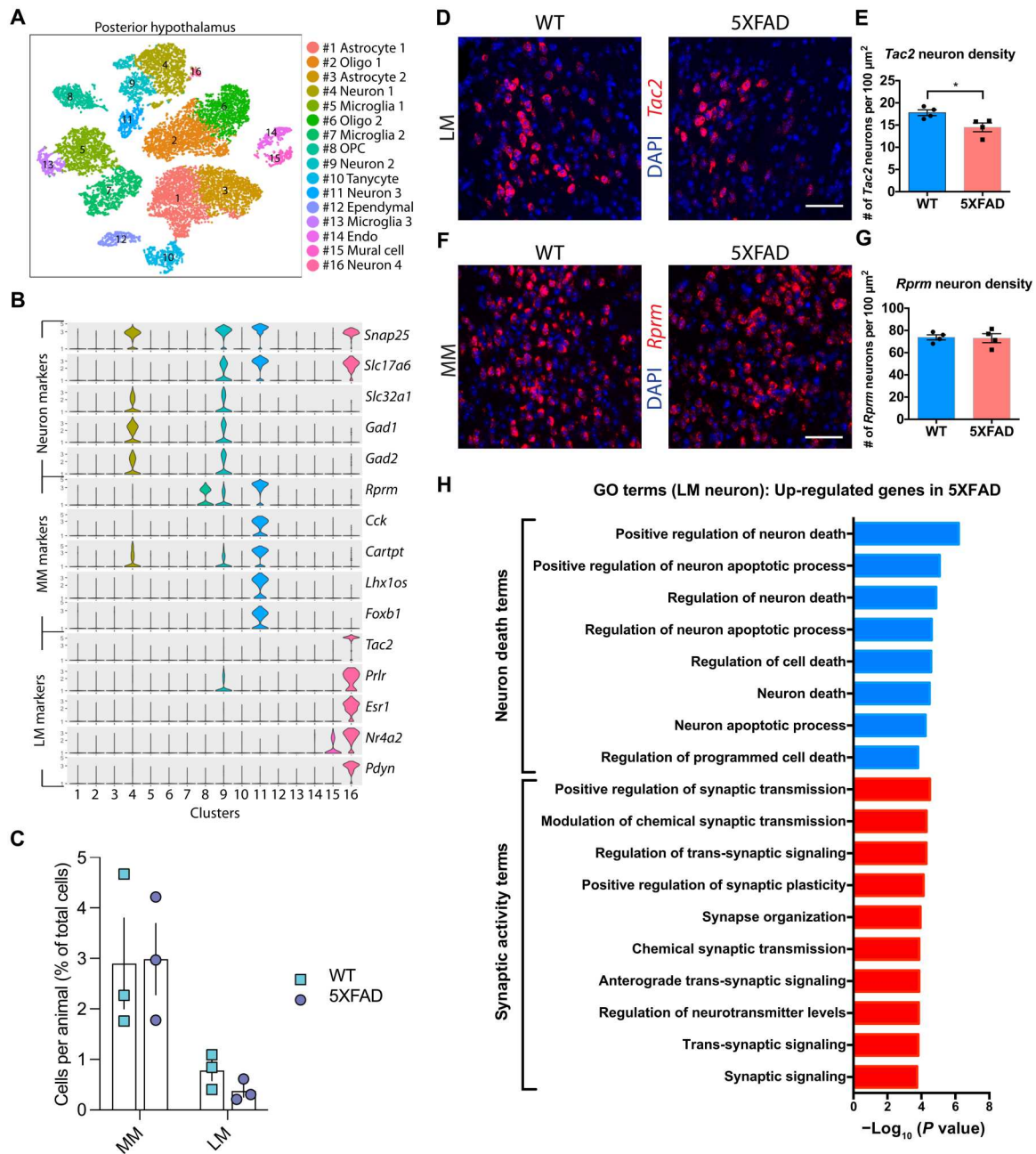


**Fig. 3. LM neurons are vulnerable to neurodegeneration in 5xFAD mice.** (A) A *t*-SNE plot shows 16 cell clusters composed of cells derived from the posterior hypothalami of brains from WT and 5xFAD mice. (B) Violin plots show markers for glutamatergic and GABAergic neurons and markers for MM neurons and LM neurons. Clusters 11 and 16 show enrichment for MM and LM markers, respectively. (C) Number of cells per hypothalamus as a percentage of total cells recovered is shown ( $n = 3$  mice per group; two-way ANOVA). (D) Confocal images show in situ hybridization of *Tac2* (red) in the LMs of WT and 5xFAD mice at 6 months of age; DAPI stain (blue). Scale bar, 50  $\mu\text{m}$ . (E) Quantification of *Tac2*-positive cells in the LMs of 6-month-old WT and 5xFAD mice.  $t(6) = 2.81$ ,  $P = 0.0308$ . \* $P < 0.05$  (unpaired *t* test).  $n = 4$  mice per genotype. (F) Confocal images show in situ hybridization of *Rprm* (red) in the MMs of WT and 5xFAD mice at 6 months of age; DAPI stain (blue). Scale bar, 50  $\mu\text{m}$ . (G) Quantification of *Rprm*-positive cells in the MMs of 6-month-old WT and 5xFAD mice.  $n = 4$  mice per genotype. (H) Gene ontology (GO) term enrichment for genes up-regulated in 5xFAD compared with WT mouse brain LM neurons (cluster 16).

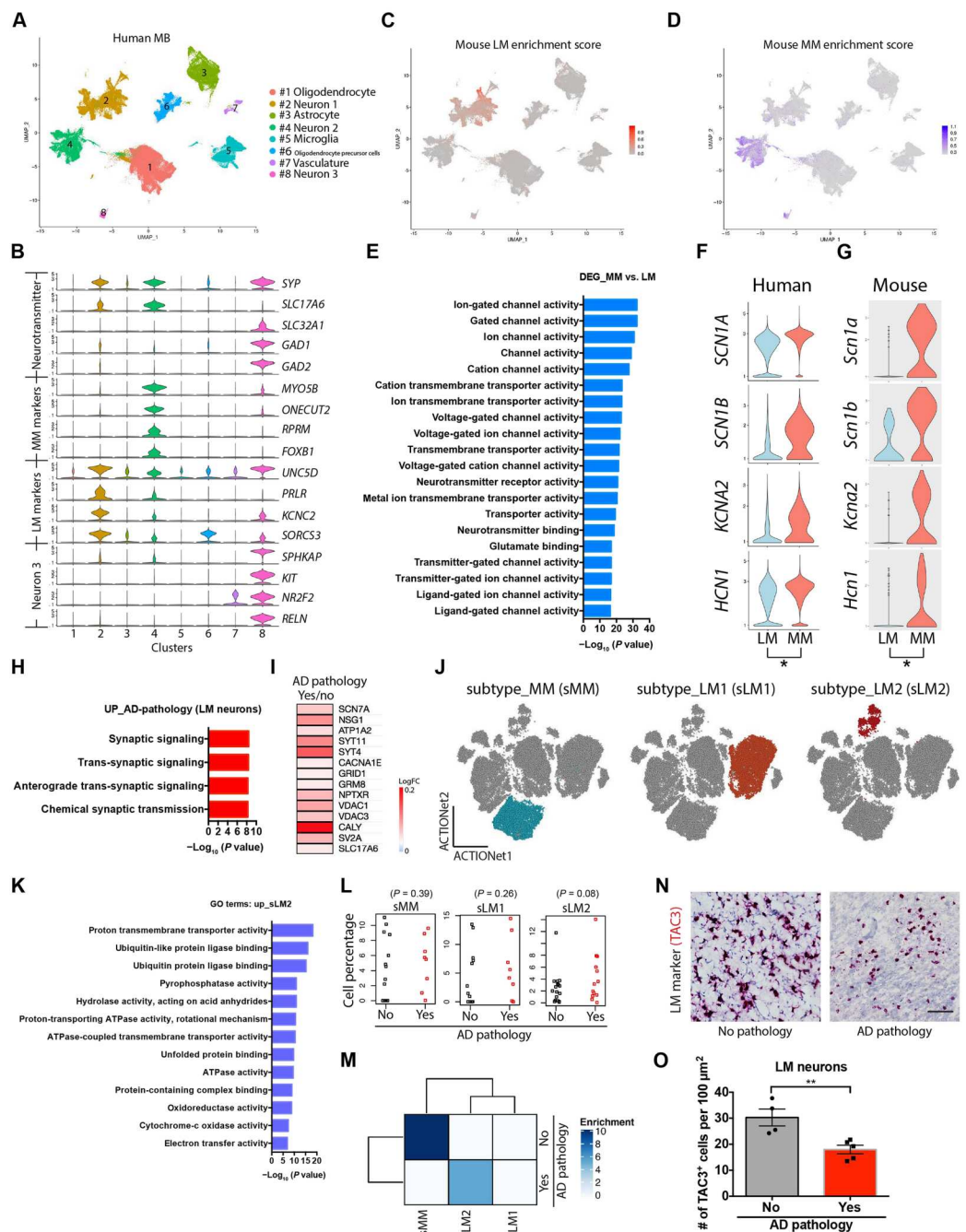
altered between genotypes (Fig. 3, F and G). We also found reduced expression of the NeuN marker in LM but not MM neurons of 6-month-old 5xFAD mice compared with WT littermates using immunohistochemistry (fig. S7). Furthermore, using stereological techniques and markers for LM and MM neurons (Tac2 and Rprm, respectively), we found reduced LM neuronal density in 6-month-old 5xFAD mice compared with age-matched WT littermates (fig. S8). Collectively, these results suggest that LM neurons

may be differentially vulnerable to neurodegeneration compared with MM neurons in 6-month-old 5xFAD mice.

To gain insights into the potential mechanisms underlying differential degeneration of LM neurons, we compared the transcriptomes of LM neurons between WT and 5xFAD mice. Enriched GO terms for genes up-regulated in 5xFAD LM neurons were related to neuronal death (including positive regulation of neuron death, neuron apoptotic process, and regulation of programmed cell

**Fig. 4. Single-nucleus transcriptomic analysis of human postmortem MB samples reveals LM and MM neurons.**

(A) Shown is a uniform manifold approximation and projection (UMAP) of single-nucleus transcriptomes in postmortem MB samples from individuals with and without AD pathology. (B) Violin plots of markers for glutamatergic and GABAergic neurons and markers for the three neuronal cell types. (C) Enrichment score analysis of human MB neurons with mouse LM neuron markers. (D) Enrichment score analysis of human MB neurons with mouse MM neuron markers. (E) Enriched GO terms for differentially expressed genes (DEGs) between human MM and LM neurons. (F and G) Violin plots showing MM and LM neuron expression of subunits of sodium and potassium ion channels and hyperpolarization-activated cyclic nucleotide-gated channels in MB samples from human (F) and mouse (G). (H) Selection of GO terms for genes up-regulated in human LM neurons in postmortem MB samples from individuals with AD pathology. (I) A heatmap showing a selection of up-regulated synaptic genes in human LM neurons in postmortem MB samples from individuals with AD pathology. (J) Shown are dimension plots indicating subtypes of human MM and LM neurons that have the most transcriptional similarity to mouse MM and LM neurons. (K) Enriched GO terms are presented for genes up-regulated in a LM neuron subcluster (sLM2, stressed LM cluster 2). (L) Shown is the percentage of cells in a human MM cluster (sMM, stressed MM) and in two LM clusters (sLM1 and sLM2) for postmortem MB samples from individuals with or without AD pathology. Wilcoxon tests were used to compare cell percentage between AD pathology and no AD pathology. (M) Overrepresentation analysis for subtypes of human MM and LM neurons (sMM, sLM1, and sLM2). Color scale indicates the significance of overrepresentation. (N) Example images of immunohistochemical staining of human postmortem MB sections from individuals with and without AD pathology showing RNA in situ hybridization of *TAC3* (red), a LM neuron marker gene. Scale bar, 50  $\mu\text{m}$ . (O) Quantification of *TAC3*<sup>+</sup> LM neurons in postmortem MB samples from individuals with and without AD pathology.  $t(7) = 3.614$ ,  $P = 0.0086$ . \*\* $P < 0.01$  (unpaired *t* test).



death) and synaptic activity (including regulation of synaptic transmission, regulation of neurotransmitter concentrations, and synaptic signaling) (Fig. 3H). We found that these terms were not enriched in MM neurons (fig. S9). To determine whether LM neuronal dysfunction was unique to MB or shared with other brain regions, we analyzed a previously published single-nucleus RNA-seq (snRNA-seq) dataset from 7-month-old mouse 5xFAD hippocampus (61). We found that genes expressed in the LM neurons were not differentially expressed in the 7-month-old 5xFAD hippocampus (fig. S10), potentially suggesting that LM neurodegeneration is associated with a unique transcriptomic state that is not necessarily associated with a brain-wide signature of neurodegeneration associated with the 5xFAD genotype.

### Single-nucleus RNA profiling of human postmortem MB samples

To explore whether MB neuron subtypes that we identified in mice are conserved in humans, we performed snRNA-seq of postmortem MB samples from 32 individuals in the Religious Orders Study or the Rush Memory and Aging Project (ROSMAP), two longitudinal cohort studies of aging and dementia. Information collected in ROSMAP cohorts included clinical data, detailed postmortem pathological evaluations, and multiomics tissue profiling (62). We selected 13 individuals with AD pathology (eight female and five male) (fig. S11A) based on multiple consensus metrics of pathology and 19 individuals as non-AD controls (11 female and 8 male). We did not observe differences in education, age of death, sex, postmortem interval, fixation interval, or comorbidities between groups (fig. S11, C to H). We confirmed that the major differences between the two groups were amyloid burden (fig. S11I) and neurofibrillary tangles (fig. S11J) based on consensus metrics quantifying pathology across multiple brain regions, including hippocampus and multiple cortical regions. Although we cannot rule out the possibility that other pathologies may have influenced our results, these findings suggest that the major differences between the pathologies of our snRNA-seq cohort were due to tau and amyloid. In total, we analyzed 136,636 nuclei in MB samples from 32 individuals, which stratified into major brain cell types, including neurons (expressing *SYT1*, *SNAP25*, and *SYP*), astrocytes (*GFAP*, *AQP4*, and *GJA1*), microglia (*CSF1R*, *CD74*, and *C3*), oligodendrocytes (*MOBP*, *MOG*, and *CNDP1*), oligodendrocyte precursor cells (*VCAN*, *MEGF11*, and *PDGFR*), and vascular cells (*FLT1*, *CLDN5*, and *PDGFRB*) (fig. S12A).

Within neurons, we identified three major neuronal cell types, of which two expressed glutamatergic markers (*SLC17A6*) and one expressed GABAergic markers (*SLC32A1*, *GAD1*, and *GAD2*) (Fig. 4, A and B). To test whether specific neuronal clusters corresponded to the LM and MM neurons that we found in mice, we calculated the enrichment score from the aggregation of the top 15 marker genes identified in the mouse LM and MM neuron clusters (fig. S13A). We found that distinct neuronal clusters corresponded to the mouse LM (Fig. 4C and fig. S13, C to E) and MM (Fig. 4D). RNA-seq of the human postmortem MB samples revealed that the mouse LM neuron marker gene *KCNC2* was expressed exclusively in LM neurons in human tissue and that the mouse MM neuron marker gene *FOXB1* was expressed exclusively in MM neurons in human tissue, indicating that mouse MM and LM neuronal marker genes are conserved in humans (fig. S14). We also identified a neuronal cell type marked by *RELN* expression, which we

confirmed using in situ hybridization (fig. S12B), that we did not observe in mouse, potentially representing a rare MB neuronal subtype that may be unique to human MB compared with mouse MB.

Mouse LM and MM neurons generated distinct firing patterns in our slice electrophysiology experiments, which were reflected by their differential expression of ion channel transcripts. Enriched GO terms for differentially expressed genes (DEGs) between human LM and MM neurons were also associated with ion channel activity (Fig. 4E). As expected, compared with human LM neurons, human MM neurons harbored higher expression of the genes encoding the subunits of ion channels, including *SCN1A*, *SCN1B*, *KCNA2*, and *HCN1* (Fig. 4, F and G), potentially suggesting that distinct spiking properties of MM and LM neurons might be conserved across mice and humans.

To determine whether human LM neurons also up-regulate genes associated with synaptic activity in individuals with AD as we observed in 5xFAD mice, we performed DEG analysis between MB samples from individuals with AD pathology and non-AD controls. Individuals with AD pathology showed up-regulation of genes related to synaptic activity in human LM neurons (Fig. 4H), such as *SCN7A* (voltage-gated sodium channel), *NSG1* (neuronal vesicle trafficking protein), *ATP1A2* [an adenosine triphosphatase (ATPase)  $\text{Na}^+/\text{K}^+$  transporter subunit], *SYT4* and *SYT11* (synaptotagmins), *CACNA1E* (voltage-gated calcium channel), *GRID1* (glutamate ionotropic receptor), *GRM8* (glutamate metabotropic receptor), *NPTXR* (neuronal pentraxin receptor), *VDAC1* and *VDAC3* (voltage-dependent anion channels), *CALY* (calcyon neuron-specific vesicular protein), *SV2A* (a synaptic vesicle glycoprotein), and *SLC17A6* (vesicular glutamate transporter) (Fig. 4I). This observation suggests that LM neurons may become more active in individuals with AD compared with non-AD controls.

To further resolve transcriptomic responses to AD in human MB samples, we identified subclusters within MM and LM neurons (Fig. 4J). LM neurons clustered into two subpopulations (Fig. 4J), one of which showed enrichment for GO terms associated with cellular stress responses (including unfolded protein binding, ubiquitin protein ligase binding, and electron transfer activity) (Fig. 4, K and L). Overrepresentation analysis revealed that individuals with AD pathology were overrepresented in this cluster (Fig. 4M). Together, these findings suggest that human LM neurons mount a unique stress-associated transcriptional response to AD compared with LM neurons. In situ hybridization of human MB samples further confirmed that individuals with AD pathology harbored increased expression of *CALY* (fig. S15) and *SYT11* (fig. S16) in the LM compared with individuals with no AD pathology. These results suggest that the LM neurons in AD individuals and 6-month-old 5xFAD mice harbored similar gene expression signatures related to neuronal hyperexcitability and cellular stress (63–65). To directly test whether LM neurons degenerate in individuals with AD, we performed RNA in situ hybridization of the LM marker gene *TAC3*, the human homolog of the rodent *Tac2*, and quantified *TAC3* cells in the postmortem MB samples of individuals with AD pathology. We found that the number of *TAC3* cells in the MB was reduced in individuals with AD pathology compared with those with no pathology (Fig. 4, N and O). These findings suggest that LM neurons exhibit degeneration in individuals with AD, similar to our observations in the 5xFAD mice.

### LM neurons of 5xFAD mice become hyperactive in an age-dependent manner

Our transcriptional findings in both mice and humans suggested that LM neurons increase neuronal firing in AD compared with MM neurons. To directly test this hypothesis, we used electrophysiology and recorded LM and MM neurons in brain slices from female 2-month-old 5xFAD mice and WT control littermates, an age that we chose because neuronal hyperactivity may occur in the early stages of the disease (12, 66). Using cell-attached patch-clamp recordings, we found that the frequency of spontaneous action potentials was increased in mouse LM neurons (Fig. 5, A and B) but not in MM neurons (Fig. 5, C and D), indicating that LM neurons exhibited increased firing in the MBs of 5xFAD mice compared with WT littermates. We also recorded spontaneous action potentials of LM neurons in brain slices from the tau P301S mouse model of AD (67), which recapitulates AD tau pathology. Similar to our findings in 5xFAD mice, LM neurons also showed increased spiking activity in tau P301S mouse brains compared with mouse brains from WT control littermates (fig. S17). To gain insights into the synaptic mechanisms underlying increased firing of LM neurons, we performed whole-cell patch-clamp recording. By measuring the spontaneous postsynaptic excitatory currents (sEPSC) in MM and LM neurons, we found that the frequency but not the amplitude of sEPSC was increased in LM neurons of 5xFAD mice (Fig. 5, E to G), whereas neither the frequency nor the amplitude of sEPSC was altered between genotypes in MM neurons (Fig. 5, H to J). These observations suggest that LM neurons in the 5xFAD mouse model may increase firing activity, in part because they receive more excitatory synaptic inputs than LM neurons of WT littermates.

To determine whether the hyperactivity of LM neurons observed in 2-month-old 5xFAD mice persists in later stages of AD, we recorded neuronal spiking in 6-month-old 5xFAD mice. We found that the frequency of spontaneous action potentials was further increased in LM neurons of 6-month-old mice compared with that of LM neurons in 2-month-old 5xFAD mice (Fig. 5K), whereas the firing frequency of MM neurons was not altered between 2 and 6 months of age (Fig. 5K). The baseline firing frequency of LM neurons in 5xFAD mice increased from ~4 Hz in 2-month-old mice to ~32 Hz in 6-month-old mice (Fig. 5K). This suggests that mouse LM neurons show increased neuronal hyperactivity in an age-dependent manner.

### LM neuronal hyperactivity drives memory deficits in mice

To determine whether LM neuron hyperactivity and memory deficits in AD are causally linked, we used a designer receptor exclusively activated by designer drug (DREADD) to increase activity in LM neurons of female C57BL/6 mice. We injected AAV8-CamKII $\alpha$ -hM3Dq into the MBs of 2-month-old C57BL/6 female mice and implanted a bilateral cannula above the LM neurons, enabling the delivery of clozapine *N*-oxide (CNO) to activate hM3Dq into the LM neurons (Fig. 6, A and B). We confirmed that hM3Dq-expressing LM neurons increased firing activity in response to bath application of CNO (Fig. 6C). Adeno-associated virus (AAV) was injected 3 weeks before the implantation of a bilateral cannula, allowing the expression of hM3Dq in the mouse MB. We started the behavioral tests 3 days after cannula implantation. We delivered CNO through the cannula to activate LM neurons 1 hour before the behavioral tests. CNO was delivered to both control and hM3Dq-expressing

mice to control for CNO-dependent behavioral effects. To assess spatial working memory, we tested spontaneous alternation in the Y-maze task (68). Control (AAV8-CamKII $\alpha$ -mCherry only) mice alternated arms during ~75% of trails, whereas the hM3Dq-expressing mice alternated in ~57% of trials (Fig. 6D). In addition, we performed trace fear conditioning. Training comprised five tone-interval-shock sequences (15-s tone + 30-s interval + 1-s shock), and fear memory recall was tested 24 hours later. hM3Dq-expressing mice showed reduced freezing compared with control mice during the recall tests (Fig. 6E). The effect of chemogenetic inhibition on memory performance was not confounded by changes in anxiety or motor activity measures, because we found no difference in freezing behavior in the pretone habituation period (fig. S18). Although we cannot rule out the possibility that non-LM neurons may have been affected by our viral strategy and contributed to memory deficits, these observations suggest that LM neuronal hyperactivity may be sufficient to induce memory deficits.

Next, we tested whether reducing activity in LM neurons of 5xFAD mice could ameliorate memory deficits. We used the anti-epileptic drug levetiracetam to attenuate the increased activity of LM neurons in female 6-month-old 5xFAD mice. Levetiracetam is known to treat seizures by reducing neuronal activity in part by binding to SV2A, a synaptic vesicle glycoprotein (69–72). We found that the expression of SV2A was elevated in individuals with AD pathology and in 5xFAD mice in the corresponding human and mouse LM neuronal clusters (Fig. 6, F and G). In situ hybridization of *Sv2a* and *Tac2* further revealed that the intensity of *Sv2a* puncta in *Tac2* neurons in the LM was increased in 6-month-old 5xFAD mice (Fig. 6, H and I). Bath application of 1  $\mu$ M levetiracetam to 5xFAD mouse brain slices reduced LM neuronal spiking activity (Fig. 6J), because the frequency of spontaneous action potentials was decreased after the application of levetiracetam (Fig. 6K). To test whether reducing LM neuronal activity rescued memory deficits in female 6-month-old 5xFAD mice, we delivered levetiracetam specifically into the LM via a bilateral cannula (Fig. 6L). We infused levetiracetam daily for 7 days before behavioral testing, and on the day of behavioral testing, levetiracetam was infused 1 hour before the tests. We again used spontaneous alternation in the Y-maze task and trace fear conditioning tests in which 5xFAD mice showed deficits by 6 months of age (19, 73). In the Y-maze task, we found that whereas 5xFAD mice receiving vehicle alternated in ~51% of the trials, less than WT control littermates receiving vehicle (~72%), 5xFAD mice receiving levetiracetam alternated in ~69% of the trials (Fig. 6M). In the trace fear conditioning tests, the freezing percentage of 5xFAD mice receiving vehicle was reduced compared with that of WT control littermates receiving vehicle, and levetiracetam rescued this deficit (Fig. 6N). In addition, we found that levetiracetam attenuated the intensity of *Sv2a* puncta in *Tac2* neurons in the LM neurons to WT levels, suggesting that the transcriptional signature relating to neuronal hyperactivity was also alleviated by levetiracetam (fig. S19). Although we cannot rule out effects of levetiracetam on other cell types, we found that levetiracetam had no effect on the firing activity of MM neurons (fig. S20), suggesting that the effect of levetiracetam on memory within the MB was due to changes in LM neurons. Together, these observations provide evidence that hyperactivity of LM neurons contributes to memory deficits and that manipulating LM neuronal activity may represent a therapeutic strategy to improve cognition in AD.



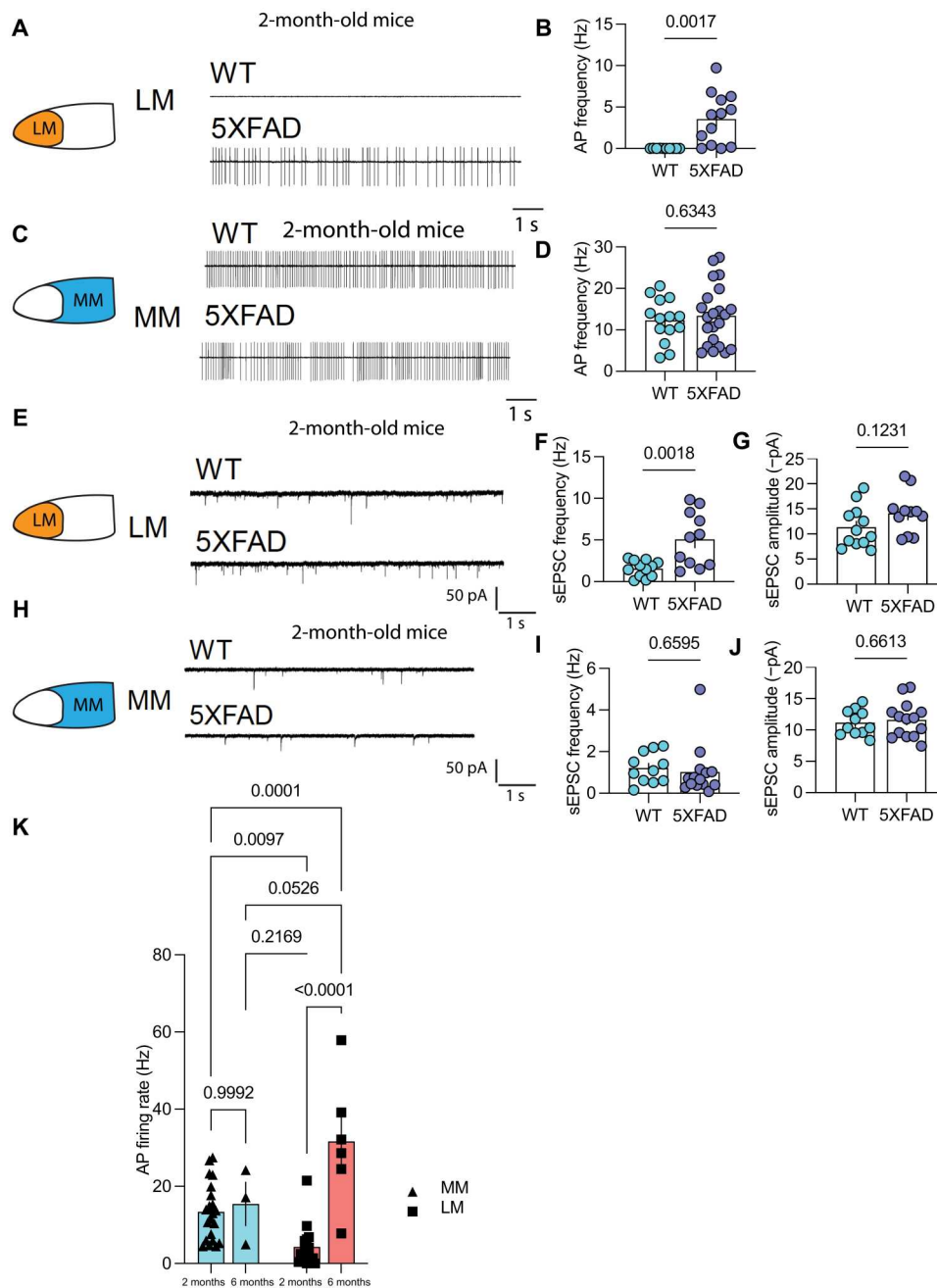
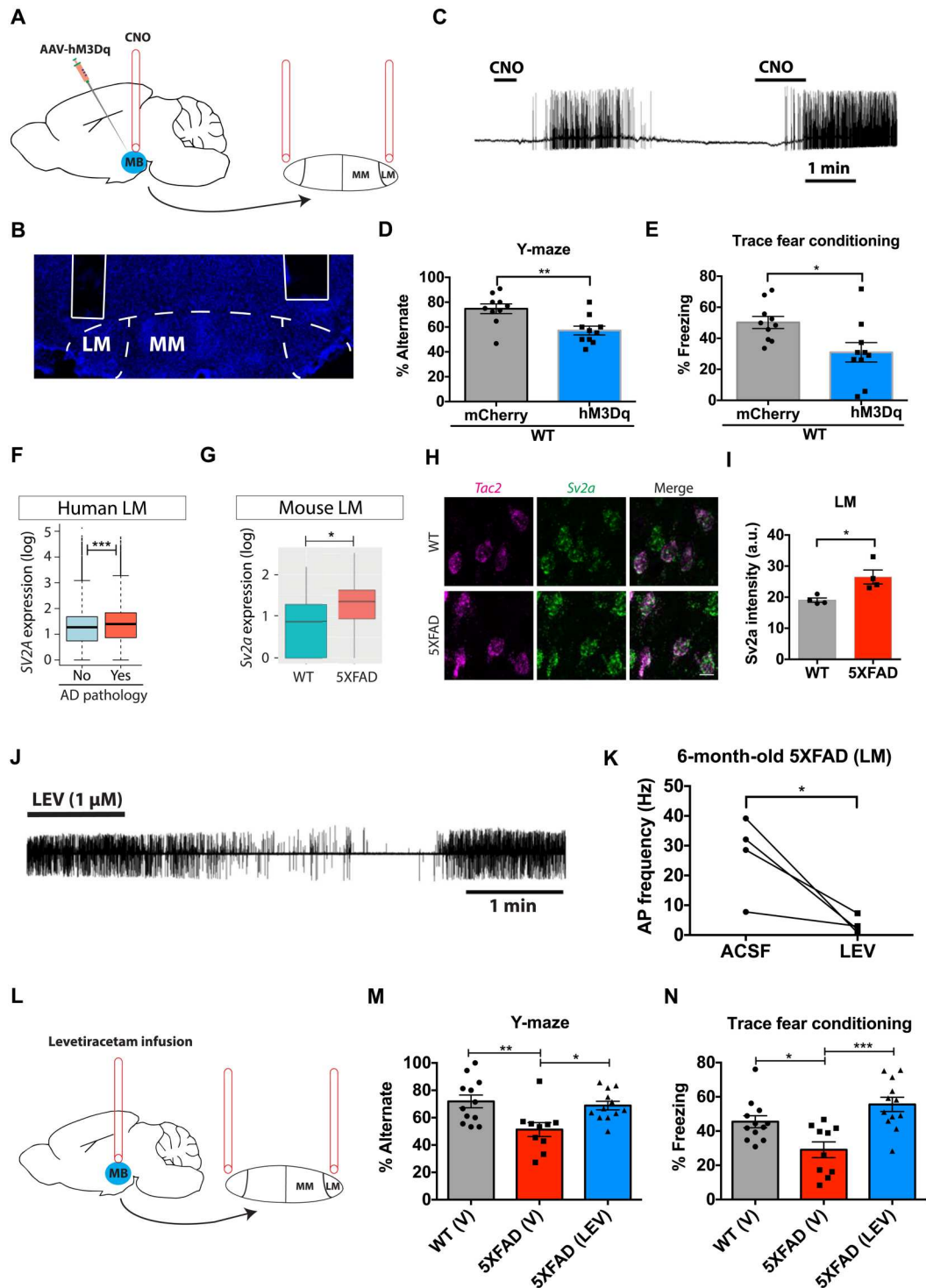


**Fig. 5. LM neurons of 5xFAD mice are hyperactive.** (A) Shown are representative AP traces of the LM neurons of a 2-month-old 5xFAD mouse and a WT littermate control using brain slice electrophysiology. (B) Shown is the summary of the firing frequency of LM neurons in a 2-month-old 5xFAD mouse and a WT littermate control.  $t(20) = 3.403$ ,  $P = 0.0017$ .  $**P < 0.01$  (unpaired  $t$  test).  $n = 9$  in the WT group and  $n = 13$  in the 5xFAD group. (C) Shown are representative AP traces from the MM neurons of a 2-month-old 5xFAD and a WT littermate control. (D) Shown is the summary of the firing frequency of MM neurons in a 2-month-old 5xFAD mouse and a WT littermate control.  $n = 14$  in the WT group and  $n = 22$  in the 5xFAD group. (E) Shown are representative traces of spontaneous excitatory postsynaptic currents (sEPSC) in the LM neurons of a 2-month-old 5xFAD mouse and a WT littermate control. (F and G) Quantification of sEPSC frequency (F) and amplitude (G) in the LM neurons of a 2-month-old 5xFAD mouse and a WT littermate control.  $t(21) = 3.57$ ,  $P = 0.0018$  (F) (unpaired  $t$  test).  $n = 12$  in the WT group and  $n = 11$  in the 5xFAD group. (H) Shown are representative traces of sEPSCs of MM neurons from a 2-month-old 5xFAD mouse and a WT littermate control. (I and J) Quantification of sEPSC frequency (I) and amplitude (J) in the MM neurons of a 2-month-old 5xFAD mouse and a WT littermate control.  $n = 11$  in the WT group and  $n = 13$  in the 5xFAD group. (K) Quantification of AP frequency in the LM and MM neurons of 2- and 6-month-old 5xFAD mice is shown. Two-way ANOVA with Šidák's post hoc test  $F_{1,14} = 6.64$ ,  $P = 0.022$  (interaction).

**Fig. 6. LM neuronal hyperactivity contributes to memory deficits in mice.**

**(A)** Experimental design for increasing neuronal activity specifically in neurons located in the LMs of mice. An AAV vector carrying the DREADD hM3Dq (Gq) was injected into the MB, and a cannula was implanted above the LM, allowing the delivery of clozapine *N*-oxide (CNO) into the mouse LM.

**(B)** A confocal image shows the location of the cannula just above the LM in mouse brain. **(C)** Shown is an AP trace induced by mouse LM neurons expressing the hM3Dq DREADD in response to 10  $\mu$ M CNO. **(D)** WT mice expressing hM3Dq showed reduced performance in the Y-maze task compared with control mice (expressing mCherry).  $t(18) = 3.319, P = 0.0038$  (unpaired *t* test).  $n = 10$  mice per group. **(E)** WT mice expressing hM3Dq showed reduced freezing time in the trace fear conditioning test compared with control mice (expressing mCherry).  $t(18) = 2.612, P = 0.0176$  (unpaired *t* test).  $n = 10$  mice per group. **(F and G)** *Sv2a* expression in (F) human LM neurons and (G) mouse LM neurons. **(H)** In situ hybridization of *Tac2* (magenta) and *Sv2a* (green) in brain sections from the LMs of a 6-month-old 5xFAD mouse and a WT littermate control. Scale bar, 10  $\mu$ m. **(I)** Quantification of *Sv2a* intensity in *Tac2*<sup>+</sup> LM neurons in a 6-month-old 5xFAD mouse and a WT littermate control.  $t(6) = 3.161, P = 0.0195$ . \* $P < 0.05$  (unpaired *t* test).  $n = 4$  mice per group. **(J)** A representative trace of spontaneous APs acquired using cell-attached patch-clamp recording in LM neurons of 5xFAD mice at 6 months of age before, during, and after bath application of levetiracetam (LEV; 1  $\mu$ M). **(K)** Quantification of AP frequency in LM neurons from 6-month-old 5xFAD mice before and after bath application of LEV or artificial cerebrospinal fluid (ACSF) as control.  $t(3) = 3.286, P = 0.0462$  (paired *t* test).  $n = 4$  neurons from three mice. **(L)** Experimental design for LEV infusion specifically into the LMs of 6-month-old 5xFAD mice. **(M)** Percentage of spontaneous alternation in the Y-maze task in WT mice treated with vehicle (V) and 6-month-old 5xFAD mice treated with vehicle or LEV.  $F_{2,31} = 6.238, P = 0.0053$  (one-way ANOVA with Tukey's post hoc test).  $n = 12$  mice in WT (V) group, 10 mice in 5xFAD (V) group, and 12 mice in 5xFAD (LEV) group. **(N)** Percentage of freezing responses from the cued trace fear conditioning test in WT mice treated with vehicle (V) and 6-month-old 5xFAD mice treated with vehicle or LEV.  $F_{2,31} = 10.35, P = 0.0004$  [one-way ANOVA with Tukey's post hoc test;  $n = 12$  mice in WT (V) group,  $n = 10$  mice in 5xFAD (V) group, and  $n = 12$  mice in 5xFAD (LEV) group. \* $P < 0.05$ ; \*\* $P < 0.01$ ; \*\*\* $P < 0.001$ ; unpaired *t* test].



Downloaded from https://www.science.org at Massachusetts Institute of Technology on June 22, 2023

## DISCUSSION

The mechanisms predisposing individual neuronal circuits to degeneration in the AD brain are poorly understood. One possibility is that aging neurons die in a stochastic, erratic manner. A competing possibility—one with critical therapeutic implications—is that specific neurons become vulnerable to degeneration in a predictable manner based on a convergence of genetic identity, anatomic connectivity, and cellular milieu. Here, we found that the MB contains two neuronal cell types with distinct molecular markers, neuronal morphologies, long-range projection targets, and electrophysiological properties. The transcriptional profiles of the two types of MB neurons were conserved across mice and humans. LM neurons up-regulated genes associated with neuronal activity in both an AD mouse model and postmortem human brain tissue with AD pathology compared with non-AD controls. LM neurons—but not MM neurons—exhibited age-dependent progression of neuronal hyperactivity in 5xFAD mice. Increasing spiking activity in LM neurons of WT mice impaired performance in two tests of memory, and selectively reducing LM neuronal hyperactivity in 5xFAD mice rescued memory deficits, suggesting that LM neuronal hyperactivity is both necessary and sufficient to drive memory deficits.

Previous studies suggest that neurodegeneration in the cerebral cortex and subiculum is not observed before 9 months of age in 5xFAD mice (19, 74). Our findings suggest that LM neurons degenerate as early as 6 months of age in 5xFAD mice, potentially one of the earliest brain regions to degenerate in this AD mouse model. These findings more broadly suggest that some neuronal types may harbor distinct cellular properties, including circuit connectivity and cell-autonomous properties, that increase their risk for dysfunction and degeneration. The asymmetric reduction of neurons in the MB may induce desynchronized circuit assembly and brain-wide network dysfunction. Loss of LM neurons may also redirect MB presynaptic inputs to the remaining LM neurons, leading to excessive synaptic connections and neuronal hyperactivity. Our data indicate that LM neurons increased spontaneous firing frequency in 5xFAD mice, suggesting that LM neurons might receive more excitatory presynaptic inputs in 5xFAD mice compared with control littermates. Given that behavioral deficits in 5xFAD mice do not emerge until ~6 months of age (19), LM neuronal hyperactivity may critically induce memory deficits. Reducing LM neuronal hyperexcitability in 6-month-old 5xFAD mice using levetiracetam rescued memory deficits. Of note, levetiracetam reduced neuronal hyperactivity in LM neurons but did not affect the firing of MM neurons, suggesting that levetiracetam may correct pathological hyperactivity without affecting physiological neuronal firing, making it a potential approach to treat AD associated with neuronal hyperactivity (75–77).

Our study has several limitations. We acknowledge that some of our behavioral data had broad overlap between groups, and therefore the subtle changes observed should be interpreted with caution. However, transcriptomic overlap between mouse and human MB neuronal populations suggests that increased neuronal activity in LM neurons may represent an inflection point in the progressive loss of memory in AD. We found up-regulation of neuronal activity in 5xFAD mouse LM neurons at 2 and 6 months of age compared with age-matched WT littermates and also found up-regulation of LM neuronal activity in tau P301S mice at 9 months of age compared with age-matched WT littermates. Additional mouse

models of AD may be helpful to further test the effects of age, genotype, and AD pathology on neuronal activity in MB neurons. In addition, although the primary goal of our study was to explore contributions of MB neuronal heterogeneity to AD pathology and memory dysfunction, we did not elucidate the cellular mechanisms linking neuronal hyperactivity to cell death. Hyperactivity may be associated with DNA damage and a cellular state leading to neuronal senescence (78). Furthermore, pinpointing how subtypes of MB neurons are coordinated within broader medial limbic memory circuits might contribute to additional insight into memory impairments in AD. Further defining hypothalamic neurons (79–83) might help to unravel the complex physiology of hypothalamic contributions to memory deficits in AD, particularly given that lesion studies suggest that the MB governs spatial working memory, navigational memory, and episodic memory (35). Future studies using transgenic mouse lines to specifically label distinct MB neuronal subtypes will enable the exploration of functional contributions of each subtype to particular aspects of learning, memory, and cognition. For example, previous studies have found head-direction and angular velocity cells in the LM (84, 85), and our study provides a strategy to test their functional contributions to specific memory processes. Collectively, our data suggest that subcortical contributions to memory may play important roles in AD and neurodegeneration.

## MATERIALS AND METHODS

### Study design

The goal of this study was to define the cellular heterogeneity of the MB in mouse brain and its possible roles in regulating memory in AD. We used scRNA-seq to define the cell types of the MB in WT mice. 5xFAD (Tg 6799) breeding pairs were acquired from the Mutant Mouse Resource and Research Center (stock no. 034848-JAX). 5xFAD mice were crossed with WT mice to generate offspring for this study. All animal experiments were conducted in accordance with National Institutes of Health guidelines and were approved by the Committee on Animal Care of the Division of Comparative Medicine at the Massachusetts Institute of Technology. Female mice were used in the study unless otherwise specified. Two-month-old WT (C57BL/6; JAX stock no. 000664) mice were used for initial scRNA-seq studies. Six-month-old 5xFAD mice and littermate controls were further used for scRNA-seq and the subsequent validation experiments. Mouse brain slices for electrophysiology were from 2- and 6-month-old 5xFAD mice and littermate controls. We performed scRNA-seq of 6-month-old 5xFAD mice versus WT littermates.

We undertook snRNA-seq in postmortem MB samples from individuals with varying stages of AD pathology. For snRNA-seq human sequencing experiments, postmortem samples were processed in batches that included both AD and non-AD pathology in case of batch effects. Our human MB dataset contained a total of 32 individuals from the ROS or the MAP, two longitudinal cohort studies of aging and dementia. These cohort studies include clinical data collected annually; detailed postmortem pathological evaluation; and extensive genetic, epigenetic, transcriptomic, proteomic, and metabolomic bulk tissue profiling (62). ROSMAP data and biospecimens can be requested at [www.radc.rush.edu](http://www.radc.rush.edu). Details of the clinical and pathological data collection methods have been previously reported (86–90). Informed

consent was obtained from each individual, and the ROSMAP studies were approved by the Institutional Review Board of Rush University Medical Center. All participants signed a repository consent to allow their data and biospecimens to be repurposed. NIA-Reagan pathological diagnosis of intermediate likelihood or high likelihood was used to identify individuals with or without AD pathology. Postmortem brain specimens in our study came from 13 individuals with AD pathology (8 female and 5 male) and 19 individuals with no AD pathology (11 female and 8 male). AD pathology and non-AD pathology groups were balanced for years of education and age of death. Inclusion criteria for AD diagnosis included multiple metrics of AD pathology.

We characterized distinct neuronal populations in the MBs of mouse and human brains using histology. On the basis of our observation that LM neurons were associated with hyperactivity in AD using slice electrophysiology and single-cell transcriptomic profiling, we manipulated LM neurons in WT and 5xFAD mice using the DREADD hM3Dq. For all studies, mice were controlled by age and sex across groups. For sequencing, immunohistochemistry, and RNAscope, all groups were processed, stained, and imaged at the same time. Imaging quantification was carried out in a blinded fashion by a researcher who did not perform the imaging, and no mice were excluded from analysis.

### Statistical analysis

Previous studies using similar experiments or power analysis were used to determine sample size. Student's *t* (two-sided) test was used for comparison between two groups (e.g., LM versus MM and WT versus 5xFAD mice). One-way analysis of variance (ANOVA) was used in experiments containing more than two groups. Tukey's post hoc tests were used where appropriate. Two-way ANOVAs were used in experiments containing two variables (genotypes and ages). All statistics, except scRNA-seq analysis, which was performed using R, were performed using GraphPad Prism, with significance set at  $P < 0.05$ . Throughout the paper, values represent means; error bars indicate SEMs; *N* refers to biological replicates. Only positive statistics were reported. All measurements and testing were performed blind to the genotypes or experimental manipulations.

### Supplementary Materials

#### This PDF file includes:

Supplementary Methods  
Figs. S1 to S20  
References (91–94)

#### Other Supplementary Material for this manuscript includes the following:

Table S1  
Data file S1  
MDAR Reproducibility Checklist

[View/request a protocol for this paper from Bio-protocol.](#)

### REFERENCES AND NOTES

- R. G. Canter, J. Penney, L.-H. Tsai, The road to restoring neural circuits for the treatment of Alzheimer's disease. *Nature* **539**, 187–196 (2016).
- W. V. Graham, A. Bonito-Oliva, T. P. Sakmar, Update on Alzheimer's disease therapy and prevention strategies. *Annu. Rev. Med.* **68**, 413–430 (2017).
- J. M. Long, D. M. Holtzman, Alzheimer disease: An update on pathobiology and treatment strategies. *Cell* **179**, 312–339 (2019).
- M. A. Busche, A. Konnerth, Neuronal hyperactivity—A key defect in Alzheimer's disease? *BioEssays* **37**, 624–632 (2015).
- J. J. Palop, L. Mucke, Network abnormalities and interneuron dysfunction in Alzheimer disease. *Nat. Rev. Neurosci.* **17**, 777–792 (2016).
- J. J. Palop, J. Chin, L. Mucke, A network dysfunction perspective on neurodegenerative diseases. *Nature* **443**, 768–773 (2006).
- B. Zott, M. A. Busche, R. A. Sperling, A. Konnerth, What happens with the circuit in Alzheimer's disease in mice and humans? *Annu. Rev. Neurosci.* **41**, 277–297 (2018).
- M. Martinez-Losa, T. E. Tracy, K. Ma, L. Verret, A. Clemente-Perez, A. S. Khan, I. Cobos, K. Ho, L. Gan, L. Mucke, M. Alvarez-Dolado, J. J. Palop, Nav1.1-overexpressing interneuron transplants restore brain rhythms and cognition in a mouse model of Alzheimer's disease. *Neuron* **98**, 75–89.e5 (2018).
- J. J. Palop, J. Chin, E. D. Roberson, J. Wang, M. T. Thwin, N. Bien-Ly, J. Yoo, K. O. Ho, G.-Q. Yu, A. Kreitzer, S. Finkbeiner, J. L. Noebels, L. Mucke, Aberrant excitatory neuronal activity and compensatory remodeling of inhibitory hippocampal circuits in mouse models of Alzheimer's disease. *Neuron* **55**, 697–711 (2007).
- L. Verret, E. O. Mann, G. B. Hang, A. M. I. Barth, I. Cobos, K. Ho, N. Devidze, E. Masliah, A. C. Kreitzer, I. Mody, L. Mucke, J. J. Palop, Inhibitory interneuron deficit links altered network activity and cognitive dysfunction in Alzheimer model. *Cell* **149**, 708–721 (2012).
- B. Zott, M. M. Simon, W. Hong, F. Unger, H.-J. Chen-Engerer, M. P. Froesch, B. Sakmann, D. M. Walsh, A. Konnerth, A vicious cycle of  $\beta$  amyloid-dependent neuronal hyperactivation. *Science* **365**, 559–565 (2019).
- M. A. Busche, X. Chen, H. A. Henning, J. Reichwald, M. Staufenbiel, B. Sakmann, A. Konnerth, Critical role of soluble amyloid- $\beta$  for early hippocampal hyperactivity in a mouse model of Alzheimer's disease. *Proc. Natl. Acad. Sci. U.S.A.* **109**, 8740–8745 (2012).
- S. D. Vann, Re-evaluating the role of the mammillary bodies in memory. *Neuropsychologia* **48**, 2316–2327 (2010).
- S. D. Vann, J. P. Aggleton, The mammillary bodies: Two memory systems in one? *Nat. Rev. Neurosci.* **5**, 35–44 (2004).
- G. Vetere, J. W. Kenney, L. M. Tran, F. Xia, P. E. Steadman, J. Parkinson, S. A. Josselyn, P. W. Frankland, Chemogenetic interrogation of a brain-wide fear memory network in mice. *Neuron* **94**, 363–374.e4 (2017).
- A. L. Wheeler, C. M. Teixeira, A. H. Wang, X. Xiong, N. Kovacevic, J. P. Lerch, A. R. McIntosh, J. Parkinson, P. W. Frankland, Identification of a functional connectome for long-term fear memory in mice. *PLoS Comput. Biol.* **9**, e1002853 (2013).
- J. P. Aggleton, A. Pralus, A. J. D. Nelson, M. Hornberger, Thalamic pathology and memory loss in early Alzheimer's disease: Moving the focus from the medial temporal lobe to Papez circuit. *Brain J. Neurol.* **139**, 1877–1890 (2016).
- R. Gail Canter, W.-C. Huang, H. Choi, J. Wang, L. Ashley Watson, C. G. Yao, F. Abdurrob, S. M. Bousleiman, J. Z. Young, D. A. Bennett, I. Delalle, K. Chung, L.-H. Tsai, 3D mapping reveals network-specific amyloid progression and subcortical susceptibility in mice. *Commun. Biol.* **2**, 360 (2019).
- H. Oakley, S. L. Cole, S. Logan, E. Maus, P. Shao, J. Craft, A. Guillozet-Bongaarts, M. Ohno, J. Disterhoff, L. Van Eldik, R. Berry, R. Vassar, Intraneuronal  $\beta$ -amyloid aggregates, neurodegeneration, and neuron loss in transgenic mice with five familial Alzheimer's disease mutations: Potential factors in amyloid plaque formation. *J. Neurosci.* **26**, 10129–10140 (2006).
- K. B. Bhattacharyya, James Wenceslaus Papez, his circuit, and emotion. *Ann. Indian Acad. Neurol.* **20**, 207–210 (2017).
- E. J. Bubb, L. Kinnavane, J. P. Aggleton, Hippocampal-diencephalic-cingulate networks for memory and emotion: An anatomical guide. *Brain Neurosci. Adv.* **1**, 2398212817723443 (2017).
- H.-L. Teuber, B. Milner, H. G. Vaughan Jr., Persistent anterograde amnesia after stab wound of the basal brain. *Neuropsychologia* **6**, 267–282 (1968).
- H. Dusoir, N. Kapur, D. P. Byrnes, S. McKinstry, R. D. Hoare, The role of diencephalic pathology in human memory disorder. Evidence from a penetrating paranasal brain injury. *Brain J. Neurol.* **113** (Pt 6), 1695–1706 (1990).
- G. A. Carlesimo, L. Serra, L. Fadda, A. Cherubini, M. Bozzali, C. Caltagirone, Bilateral damage to the mamillo-thalamic tract impairs recollection but not familiarity in the recognition process: a single case investigation. *Neuropsychologia* **45**, 2467–2479 (2007).
- D. Tsivilis, S. D. Vann, C. Denby, N. Roberts, A. R. Mayes, D. Montaldi, J. P. Aggleton, A disproportionate role for the fornix and mammillary bodies in recall versus recognition memory. *Nat. Neurosci.* **11**, 834–842 (2008).
- S. D. Vann, D. Tsivilis, C. E. Denby, J. R. Quamme, A. P. Yonelinas, J. P. Aggleton, D. Montaldi, A. R. Mayes, Impaired recollection but spared familiarity in patients with extended hippocampal system damage revealed by 3 convergent methods. *Proc. Natl. Acad. Sci. U.S.A.* **106**, 5442–5447 (2009).

27. R. S. Rosenbaum, F. Gao, K. Honjo, C. Raybaud, R. K. Olsen, D. J. Palombo, B. Levine, S. E. Black, Congenital absence of the mammillary bodies: A novel finding in a well-studied case of developmental amnesia. *Neuropsychologia* **65**, 82–87 (2014).
28. J. Tedder, L. Miller, S. Tu, M. Hornberger, S. Lah, Into the future with little past: exploring mental time travel in a patient with damage to the mammillary bodies/fornix. *Clin. Neuropsychol.* **30**, 351–366 (2016).
29. J. P. Aggleton, M. Mishkin, Mammillary-body lesions and visual recognition in monkeys. *Exp. Brain Res.* **58**, 190–197 (1985).
30. E. J. Holmes, S. Jacobson, B. M. Stein, N. Butters, Ablations of the mammillary nuclei in monkeys: Effects on postoperative memory. *Exp. Neurol.* **81**, 97–113 (1983).
31. A. Parker, D. Gaffan, Mammillary body lesions in monkeys impair object-in-place memory: Functional unity of the fornix-mammillary system. *J. Cogn. Neurosci.* **9**, 512–521 (1997).
32. J. P. Aggleton, N. Neave, S. Nagle, P. R. Hunt, A comparison of the effects of anterior thalamic, mammillary body and fornix lesions on reinforced spatial alternation. *Behav. Brain Res.* **68**, 91–101 (1995).
33. T. D. Field, J. Rosenstock, E. C. King, E. Greene, Behavioral role of the mammillary efferent system. *Brain Res. Bull.* **3**, 451–456 (1978).
34. E. A. Gaffan, D. M. Bannerman, E. C. Warburton, J. P. Aggleton, Rats' processing of visual scenes: Effects of lesions to fornix, anterior thalamus, mammillary nuclei or the retrohippocampal region. *Behav. Brain Res.* **121**, 103–117 (2001).
35. N. Neave, S. Nagle, J. P. Aggleton, Evidence for the involvement of the mammillary bodies and cingulum bundle in allocentric spatial processing by rats. *Eur. J. Neurosci.* **9**, 941–955 (1997).
36. A. J. D. Nelson, S. D. Vann, Mammillothalamic tract lesions disrupt tests of visuo-spatial memory. *Behav. Neurosci.* **128**, 494–503 (2014).
37. J. Rosenstock, T. D. Field, E. Greene, The role of mammillary bodies in spatial memory. *Exp. Neurol.* **55**, 340–352 (1977).
38. V. Sziklas, M. Petrides, Memory impairments following lesions to the mammillary region of the rat. *Eur. J. Neurosci.* **5**, 525–540 (1993).
39. S. D. Vann, Dismantling the Papez circuit for memory in rats. *eLife* **2**, e00736 (2013).
40. S. D. Vann, J. P. Aggleton, Evidence of a spatial encoding deficit in rats with lesions of the mammillary bodies or mammillothalamic tract. *J. Neurosci.* **23**, 3506–3514 (2003).
41. D. J. Beracochea, R. Jaffard, Effects of ibotenic lesions of mammillary bodies on spontaneous and rewarded spatial alternation in mice. *J. Cogn. Neurosci.* **2**, 133–140 (1990).
42. D. J. Béracochéa, R. Jaffard, Impairment of spontaneous alternation behavior in sequential test procedures following mammillary body lesions in mice: Evidence for time-dependent interference-related memory deficits. *Behav. Neurosci.* **101**, 187–197 (1987).
43. D. J. Béracochéa, R. Jaffard, The effects of mammillary body lesions on delayed matching and delayed non-matching to place tasks in the mice. *Behav. Brain Res.* **68**, 45–52 (1995).
44. A. Célérier, C. Pierard, D. Beracochea, Effects of ibotenic acid lesions of the dorsal hippocampus on contextual fear conditioning in mice: Comparison with mammillary body lesions. *Behav. Brain Res.* **151**, 65–72 (2004).
45. D. Grossi, O. L. Lopez, A. J. Martinez, Mammillary bodies in Alzheimer's disease. *Acta Neurol. Scand.* **80**, 41–45 (1989).
46. T. McDuff, S. M. Sumi, Subcortical degeneration in Alzheimer's disease. *Neurology* **35**, 123–126 (1985).
47. A. Stief, Über die anatomischen Grundlagen der vegetativen Störungen bei Geisteskrankheiten. *Dtsch. Z. Für Nervenheilkd.* **97**, 112–132 (1927).
48. S. J. Baloyannis, I. Mavroudis, I. S. Baloyannis, V. G. Costa, Mammillary bodies in Alzheimer's disease: A Golgi and electron microscope study. *Am. J. Alzheimers Dis. Demen.* **31**, 247–256 (2016).
49. B. R. Copenhaver, L. A. Rabin, A. J. Saykin, R. M. Roth, H. A. Wishart, L. A. Flashman, R. B. Santulli, T. L. McHugh, A. C. Mamourian, The fornix and mammillary bodies in older adults with Alzheimer's disease, mild cognitive impairment, and cognitive complaints: A volumetric MRI study. *Psychiatry Res.* **147**, 93–103 (2006).
50. P. Blandina, L. Munari, G. Provensi, M. B. Passani, Histamine neurons in the tuberomammillary nucleus: A whole center or distinct subpopulations? *Front. Syst. Neurosci.* **6**, 33 (2012).
51. G. V. Allen, D. A. Hopkins, Topography and synaptology of mammillary body projections to the mesencephalon and pons in the rat. *J. Comp. Neurol.* **301**, 214–231 (1990).
52. A. Gonzalo-Ruiz, L. Morte, J. M. Sanz, Glutamate/aspartate and leu-enkephalin immunoreactivity in mammillothalamic projection neurons of the rat. *Brain Res. Bull.* **47**, 565–574 (1998).
53. K. Y. Chan, M. J. Jang, B. B. Yoo, A. Greenbaum, N. Ravi, W.-L. Wu, L. Sánchez-Guardado, C. Lois, S. K. Mazmanian, B. E. Deverman, V. Gradinaru, Engineered AAVs for efficient noninvasive gene delivery to the central and peripheral nervous systems. *Nat. Neurosci.* **20**, 1172–1179 (2017).
54. T. P. Miettinen, M. Björklund, Cellular allometry of mitochondrial functionality establishes the optimal cell size. *Dev. Cell* **39**, 370–382 (2016).
55. M. Pende, S. C. Kozma, M. Jaquet, V. Oorschot, R. Burcelin, Y. Le Marchand-Brustel, J. Klumperman, B. Thorens, G. Thomas, Hypoinsulinaemia, glucose intolerance and diminished beta-cell size in S6K1-deficient mice. *Nature* **408**, 994–997 (2000).
56. G. J. Kress, S. Mennerick, Action potential initiation and propagation: Upstream influences on neurotransmission. *Neuroscience* **158**, 211–222 (2009).
57. J. A. Cruce, An autoradiographic study of the descending connections of the mammillary nuclei of the rat. *J. Comp. Neurol.* **176**, 631–644 (1977).
58. M. Seki, K. Zyo, Anterior thalamic afferents from the mammillary body and the limbic cortex in the rat. *J. Comp. Neurol.* **229**, 242–256 (1984).
59. R. B. Veazey, D. G. Amaral, W. M. Cowan, The morphology and connections of the posterior hypothalamus in the cynomolgus monkey (*Macaca fascicularis*). II. Efferent connections. *J. Comp. Neurol.* **207**, 135–156 (1982).
60. K. Stoeckel, M. Schwab, H. Thoenen, Role of gangliosides in the uptake and retrograde axonal transport of cholera and tetanus toxin as compared to nerve growth factor and wheat germ agglutinin. *Brain Res.* **132**, 273–285 (1977).
61. N. Habib, C. McCabe, S. Medina, M. Varshavsky, D. Kitsberg, R. Dvir-Szternfeld, G. Green, D. Dionne, L. Nguyen, J. L. Marshall, F. Chen, F. Zhang, T. Kaplan, A. Regev, M. Schwartz, Disease-associated astrocytes in Alzheimer's disease and aging. *Nat. Neurosci.* **23**, 701–706 (2020).
62. D. A. Bennett, A. S. Buchman, P. A. Boyle, L. L. Barnes, R. S. Wilson, J. A. Schneider, Religious Orders Study and Rush Memory and Aging Project. *J. Alzheimers Dis.* **64**, S161–S189 (2018).
63. E. Lezi, R. H. Swerdlow, Mitochondria in neurodegeneration. *Adv. Exp. Med. Biol.* **942**, 269–286 (2012).
64. R. K. Leak, Heat shock proteins in neurodegenerative disorders and aging. *J. Cell Commun. Signal.* **8**, 293–310 (2014).
65. S. Fulda, A. M. Gorman, O. Hori, A. Samali, Cellular stress responses: Cell survival and cell death. *Int. J. Cell Biol.* **2010**, 214074 (2010).
66. K. A. Vossel, A. J. Beagle, G. D. Rabinovici, H. Shu, S. E. Lee, G. Naasan, M. Hegde, S. B. Cornes, M. L. Henry, A. B. Nelson, W. W. Seeley, M. D. Geschwind, M. L. Gorno-Tempini, T. Shih, H. E. Kirsch, P. A. Garcia, B. L. Miller, L. Mucke, Seizures and epileptiform activity in the early stages of Alzheimer disease. *JAMA Neurol.* **70**, 1158–1166 (2013).
67. Y. Yoshiyama, M. Higuchi, B. Zhang, S.-M. Huang, N. Iwata, T. C. Saido, J. Maeda, T. Suhara, J. Q. Trojanowski, V. M.-Y. Lee, Synapse loss and microglial activation precede tangles in a P301S tauopathy mouse model. *Neuron* **53**, 337–351 (2007).
68. A.-K. Kraeuter, P. C. Guest, Z. Sarnyai, The Y-maze for assessment of spatial working and reference memory in mice. *Methods Mol. Biol.* **1916**, 105–111 (2019).
69. B. Abou-Khalil, Levetiracetam in the treatment of epilepsy. *Neuropsychiatr. Dis. Treat.* **4**, 507–523 (2008).
70. L. S. Deshpande, R. J. Delorenzo, Mechanisms of levetiracetam in the control of status epilepticus and epilepsy. *Front. Neurol.* **5**, 11 (2014).
71. B. A. Lynch, N. Lambeng, K. Nocka, P. Kensel-Hammes, S. M. Bajjalieh, A. Matagne, B. Fuks, The synaptic vesicle protein SV2A is the binding site for the antiepileptic drug levetiracetam. *Proc. Natl. Acad. Sci. U.S.A.* **101**, 9861–9866 (2004).
72. C. Vogl, S. Mochida, C. Wolff, B. J. Whalley, G. J. Stephens, The synaptic vesicle glycoprotein 2A ligand levetiracetam inhibits presynaptic Ca<sup>2+</sup> channels through an intracellular pathway. *Mol. Pharmacol.* **82**, 199–208 (2012).
73. M. Ohno, L. Chang, W. Tseng, H. Oakley, M. Citron, W. L. Klein, R. Vassar, J. F. Disterhoft, Temporal memory deficits in Alzheimer's mouse models: Rescue by genetic deletion of BACE1. *Eur. J. Neurosci.* **23**, 251–260 (2006).
74. W. A. Eimer, R. Vassar, Neuron loss in the 5XFAD mouse model of Alzheimer's disease correlates with intraneuronal A $\beta$ 42 accumulation and Caspase-3 activation. *Mol. Neurodegener.* **8**, 2 (2013).
75. A. Bakker, M. S. Albert, G. Krauss, C. L. Speck, M. Gallagher, Response of the medial temporal lobe network in amnesic mild cognitive impairment to therapeutic intervention assessed by fMRI and memory task performance. *NeuroImage Clin.* **7**, 688–698 (2015).
76. A. Bakker, G. L. Krauss, M. S. Albert, C. L. Speck, L. R. Jones, C. E. Stark, M. A. Yassa, S. S. Bassett, A. L. Shelton, M. Gallagher, Reduction of hippocampal hyperactivity improves cognition in amnesic mild cognitive impairment. *Neuron* **74**, 467–474 (2012).
77. P. E. Sanchez, L. Zhu, L. Verret, K. A. Vossel, A. G. Orr, J. R. Cirrito, N. Devidze, K. Ho, G.-Q. Yu, J. J. Palop, L. Mucke, Levetiracetam suppresses neuronal network dysfunction and reverses synaptic and cognitive deficits in an Alzheimer's disease model. *Proc. Natl. Acad. Sci. U.S.A.* **109**, E2895–E2903 (2012).
78. G. M. Welch, C. A. Boix, E. Schmauch, J. Davila-Velderrain, M. B. Victor, V. Dileep, P. L. Bozzelli, Q. Su, J. D. Cheng, A. Lee, N. S. Leary, A. R. Pfening, M. Kellis, L.-H. Tsai, Neurons burdened by DNA double-strand breaks incite microglia activation through antiviral-like signaling in neurodegeneration. *Sci. Adv.* **8**, eabo4662 (2022).
79. J. N. Campbell, E. Z. Macosko, H. Fenselau, T. H. Pers, A. Lyubetskaya, D. Tenen, M. Goldman, A. M. J. Versteegen, J. M. Resch, S. A. McCarroll, E. D. Rosen, B. B. Lowell, L. T. Tsai, A molecular

- census of arcuate hypothalamus and median eminence cell types. *Nat. Neurosci.* **20**, 484–496 (2017).
80. R. Chen, X. Wu, L. Jiang, Y. Zhang, Single-cell RNA-seq reveals hypothalamic cell diversity. *Cell Rep.* **18**, 3227–3241 (2017).
81. D.-W. Kim, Z. Yao, L. T. Graybuck, T. K. Kim, T. N. Nguyen, K. A. Smith, O. Fong, L. Yi, N. Koulena, N. Pierson, S. Shah, L. Lo, A.-H. Pool, Y. Oka, L. Pachter, L. Cai, B. Tasic, H. Zeng, D. J. Anderson, Multimodal analysis of cell types in a hypothalamic node controlling social behavior. *Cell* **179**, 713–728.e17 (2019).
82. L. E. Mickelsen, M. Bolisetty, B. R. Chimileski, A. Fujita, E. J. Beltrami, J. T. Costanzo, J. R. Naparstek, P. Robson, A. C. Jackson, Single-cell transcriptomic analysis of the lateral hypothalamic area reveals molecularly distinct populations of inhibitory and excitatory neurons. *Nat. Neurosci.* **22**, 642–656 (2019).
83. R. A. Romanov, A. Zeisel, J. Bakker, F. Girach, A. Hellyszay, R. Tomer, A. Alpár, J. Mulder, F. Clotman, E. Keimpema, B. Hsueh, A. K. Crow, H. Martens, C. Schwinding, D. Calvigioni, J. S. Bains, Z. Máté, G. Szabó, Y. Yanagawa, M.-D. Zhang, A. Rendeiro, M. Farlik, M. Uhlén, P. Wulff, C. Bock, C. Broberger, K. Deisseroth, T. Hökfelt, S. Linnarsson, T. L. Horvath, T. Harkany, Molecular interrogation of hypothalamic organization reveals distinct dopamine neuronal subtypes. *Nat. Neurosci.* **20**, 176–188 (2017).
84. R. W. Stackman, J. S. Taube, Firing properties of rat lateral mammillary single units: Head direction, head pitch, and angular head velocity. *J. Neurosci.* **18**, 9020–9037 (1998).
85. H. T. Blair, J. Cho, P. E. Sharp, Role of the lateral mammillary nucleus in the rat head direction circuit: A combined single unit recording and lesion study. *Neuron* **21**, 1387–1397 (1998).
86. D. A. Bennett, R. S. Wilson, J. A. Schneider, D. A. Evans, L. A. Beckett, N. T. Aggarwal, L. L. Barnes, J. H. Fox, J. Bach, Natural history of mild cognitive impairment in older persons. *Neurology* **59**, 198–205 (2002).
87. D. A. Bennett, R. S. Wilson, J. A. Schneider, D. A. Evans, N. T. Aggarwal, S. E. Arnold, E. J. Cochran, E. Berry-Kravis, J. L. Bienias, Apolipoprotein E  $\epsilon$ 4 allele, AD pathology, and the clinical expression of Alzheimer's disease. *Neurology* **60**, 246–252 (2003).
88. D. A. Bennett, J. A. Schneider, R. S. Wilson, J. L. Bienias, S. E. Arnold, Neurofibrillary tangles mediate the association of amyloid load with clinical Alzheimer disease and level of cognitive function. *Arch. Neurol.* **61**, 378–384 (2004).
89. D. A. Bennett, J. A. Schneider, N. T. Aggarwal, Z. Arvanitakis, R. C. Shah, J. F. Kelly, J. H. Fox, E. J. Cochran, D. Arends, A. D. Treinkman, R. S. Wilson, Decision rules guiding the clinical diagnosis of Alzheimer's disease in two community-based cohort studies compared to standard practice in a clinic-based cohort study. *Neuroepidemiology* **27**, 169–176 (2006).
90. D. A. Bennett, J. A. Schneider, Z. Arvanitakis, J. F. Kelly, N. T. Aggarwal, R. C. Shah, R. S. Wilson, Neuropathology of older persons without cognitive impairment from two community-based studies. *Neurology* **66**, 1837–1844 (2006).
91. A. Butler, P. Hoffman, P. Smibert, E. Papalexi, R. Satija, Integrating single-cell transcriptomic data across different conditions, technologies, and species. *Nat. Biotechnol.* **36**, 411–420 (2018).
92. H. Mathys, J. Davila-Velderrain, Z. Peng, F. Gao, S. Mohammadi, J. Z. Young, M. Menon, L. He, F. Abdurrob, X. Jiang, A. J. Martorell, R. M. Ransohoff, B. P. Hafler, D. A. Bennett, M. Kellis, L.-H. Tsai, Single-cell transcriptomic analysis of Alzheimer's disease. *Nature* **570**, 332–337 (2019).
93. T. Stuart, A. Butler, P. Hoffman, C. Hafemeister, E. Papalexi, W. M. Mauck, Y. Hao, M. Stoerckius, P. Smibert, R. Satija, Comprehensive integration of single-cell data. *Cell* **177**, 1888–1902.e21 (2019).
94. S. Mohammadi, J. Davila-Velderrain, M. Kellis, A multiresolution framework to characterize single-cell state landscapes. *Nat. Commun.* **11**, 5399 (2020).

**Acknowledgments:** We thank the study participants and staff of the Rush Alzheimer's Disease Center. We thank all members of the Tsai laboratory for technical assistance and helpful comments. **Funding:** This research was supported in part by the JBP Foundation; Ludwig Family Foundation; and National Institutes of Health (NIH) grants RF1AG054321, RF1AG062377, RF1AG054012, U01NS110453, R01AG062335, and R01AG058002 (to L.-H.T.); P30AG10161, R01AG15819, and R01AG1717 (to D.A.B.); and RF1AG054012, U01NS110453, R01AG062335, and R01AG058002 (to M.K.). **Author contributions:** W.-C.H. and L.-H.T. conceived the study. W.-C.H., M.H.M., and Z.P. designed the study and collected the data. L.L. performed and analyzed the brain slice electrophysiological experiments. W.-C.H. performed the mouse experiments with help from M.C., Z.P., X.J., H.M., M.H.M., and F.A. W.-C.H. analyzed the mouse scRNA-seq data with help from H.M., X.J., and F.G. W.-C.H. and J.D.-V. analyzed the human snRNA-seq data with help from X.J., A.P.N., and H.M. D.A.B. provided the human postmortem brain tissue samples with clinical and pathologic data and critically reviewed the manuscript. M.K. and L.-H.T. supervised the study. W.-C.H., M.H.M., Z.P., and L.-H.T. wrote the paper with critical input from all the authors. **Competing interests:** D.A.B. serves on the scientific advisory boards of AbbVie, Takeda, Origen Inc., and Vigorous Minds. M.K. serves on the scientific advisory board of the NSF-Simons Center for Multiscale Cell Fate Research (CMCF). L.-H.T. serves on the scientific advisory boards of Cognito Therapeutics, Souvien Therapeutics, Cell Signaling Technology, 4M Therapeutics, Metro Bio LLC, and Jupiter Neurosciences Inc. All other authors declare that they have no competing interests. **Data and materials availability:** All data associated with this study are present in the paper or the Supplementary Materials. Mouse MB sequencing data can be found in GEO with accession code GSE224647. Human MB sequencing data can be found in Synapse at [www.synapse.org/#!Synapse:syn50670858](http://www.synapse.org/#!Synapse:syn50670858) using the SynID syn50670858. Code used to prepare the processed counts from the raw reads and differential gene expression analysis can be accessed at Zenodo with accession number 7787348.

Submitted 17 March 2022  
Resubmitted 22 August 2022  
Accepted 31 March 2023  
Published 19 April 2023  
10.1126/scitranslmed.abq1019

## Lateral mammillary body neurons in mouse brain are disproportionately vulnerable in Alzheimer's disease

Wen-Chin Huang, Zhuyu Peng, Mitchell H. Murdock, Liwang Liu, Hansruedi Mathys, Jose Davila-Velderrain, Xueqiao Jiang, Maggie Chen, Ayesha P. Ng, TaeHyun Kim, Fatema Abdurrob, Fan Gao, David A. Bennett, Manolis Kellis, and Li-Huei Tsai

*Sci. Transl. Med.*, **15** (692), eabq1019.  
DOI: 10.1126/scitranslmed.abq1019

### View the article online

<https://www.science.org/doi/10.1126/scitranslmed.abq1019>

### Permissions

<https://www.science.org/help/reprints-and-permissions>

Use of this article is subject to the [Terms of service](#)